MDPI

Article

Extraction and Characterization of Silica from Empty Palm Fruit Bunch (EPFB) Ash

Ebitei Sintei Nelson [1,*], Sunny Iyuke [1], Michael Olawale Daramola [2] and Akindele Okewale [3]

[1] School of Chemical and Metallurgical Engineering, Faculty of Engineering and the Built Environment, University of the Witwatersrand, Johannesburg 2050, South Africa
[2] Department of Chemical Engineering, Faculty of Engineering, Built Environment and Information Technology, University of Pretoria, Hatfield, Pretoria 0028, South Africa
[3] Department of Chemical Engineering, Federal University of Petroleum Resources, Effurun (FUPRE), Warri 330102, Nigeria
* Correspondence: ebitei4nelson@yahoo.com

Abstract: Recently, there has been so much interest in using biomass waste for bio-based products. Nigeria is one of the countries with an extensive availability of palm biomass. During palm oil production, an empty palm fruit bunch (biomass) is formed, and a lot of ash is generated. This study aimed to extract and characterize silica from empty palm fruit bunch (EPFB) ash using the thermochemical method. The results show that EPFB ash contains a large amount of biogenic silica in its amorphous form. It could be extracted for further use via calcination at different temperatures and compared effectively to other biomass materials, such as rice husk ash, sugarcane bagasse, and cassava periderm. The extracted silica was characterized using XRF, XRD, TGA, SEM, and FTIR, revealing the highest silica concentration of 49.94% obtained at a temperature of 800 °C. The XRF analysis showed 99.44 wt.% pure silica, while the XRD spectrum showed that the silica in EPFB is inherently amorphous. As is evident from the study, silica obtained from EPFB ash is a potential source of silica and it is comparable to the commercial silica. Thus, it is potentially usable as a support for catalysts, in the development of zeolite-based catalysts and as an adsorbent.

Keywords: biomass waste; pyrolyzed ash; silica; calcination; amorphous phase

1. Introduction

Studies have shown that bio-oil upgrading via existing routes (thermochemical, biochemical, and physicochemical processes) accounts for most of the total biofuel production costs [1]. According to Wang et al. [2], thermochemical treatment processes can change the properties and compositions of bio-oil using heat, pressure, hydrogen, and catalysts. The extraction of silicon dioxide in this study had the tentative aim of achieving an alternative biomass source of SiO_2 from empty palm fruit bunch (EPFB) biomass to produce zeolite catalysts, an essential requirement in the thermochemical upgrading of bio-oil. EPFB biomass generated at approximately 23% per ton of fresh palm fruit bunch processed is the primary solid waste from palm oil production [3]. The main chemical composition of EPFB ash is silica, similar to the raw materials typically used in producing zeolites and other industrial processes [4]. Commercial silica and other alternative sources of silica are commonly used as catalyst support or in the synthesis of zeolite-based catalysts, usually defined according to their Si/Al ratio [5].

Silica in its amorphous form (natural or synthetic) is a specialty chemical that has a wide range of uses in industries, including catalysis, wastewater treatment, cosmetics, pharmaceutics, etc., due to its textural and morphological features, high thermal stability and mechanical strength, and low toxicity [6]. The precipitated silica segment holds a significant share in silica production and is expected to increase in 2022–2030, owing to rising demand from various industries [7].

The recovery of amorphous silica from EPFB ash could be one of the most economical sources of silica because EPFB is abundant and accounts for a significant percentage of palm oil processing waste [8,9]. EPFB ash contains a high proportion of biogenic silica in its amorphous form, which could be extracted via calcination at various temperatures for further use [6,9]. EPFB ash as a source of silica compares well to other biomass materials, such as rice husk ash, sugarcane bagasse, cassava periderm, etc. This work successfully produced synthetic amorphous silica (SiO_2) with very low residual carbon content from EPFB ash. Combustion at 800 °C improved carbon burnout in the siliceous ash product, and the produced silica was amorphous, with no spatial order of atoms and no associated hazards. The EPFB ash contained approximately 87–98% silicon dioxide (SiO_2), depending on the palm species and the region from which it was harvested [10,11]. The pyrolysis of bio-oil from empty palm fruit bunches leaves large amounts of waste ash in landfills. The ash poses a disposal problem as it is not economically used to produce valuable materials [3,12]. The waste ash also requires less water for activation, making it economical to process. Its economic use is one primary waste management option; however, EPFB ash is underutilized. Consequently, the reutilization of EPFB-pyrolyzed ash could minimize the waste disposal problem and reduce environmental pollution [9]. Therefore, it is crucial to develop a method to recycle EPFB waste ash, as it is cost-effective, abundant, and highly processable.

Pyrolyzed EPFB ash also contains trace amounts of metallic impurities that need to be removed and a measurable amount of silica that, if extracted under the right conditions, could be valuable for zeolite [13,14]. Amorphous silica is generally produced from sodium silicate, using a lot of energy to melt silica sand, and from agricultural waste, using various methods such as calcination, leaching, and acid treatments [14,15]. There is a pressing need to find a less expensive and ecologically benign silica precursor, given the rise in demand for readily available, pricey zeolite catalysts with a complex manufacturing process and environmental contamination [16]. The search for these alternate silica sources is crucial since synthesizing zeolites from chemical reagents is costly [17]. The hydrothermal synthesis method often utilized to produce zeolite catalysts is the most widely used in zeolite synthesis. In this method, the raw materials are dissolved in aqueous alkaline solvents to achieve high product yields at relatively low crystallization temperatures and short crystallization times without needing an organic template [18].

Previous studies have focused on using renewable raw materials in an environmentally friendly manner to replace the silicate product of the quartz melt. Generally, silicate has been successfully extracted from agricultural wastes without the necessary use of templates, focusing on rice husk [19,20], corn cob [21,22], sugarcane bagasse [23–26], palm kernel ash [27], and cassava periderm [28]. According to Utama et al. [29], the best extraction conditions were 50 min, a sodium hydroxide concentration of 1.40 N, and a volume ratio of ash to solvent of 0.23. Samat et al. [13], investigated the bio-silica content of EPFB and PKS and their properties as a function of calcination temperatures. They reported that reasonable amounts of silica were only available for all samples at higher temperatures, and EPFB achieved the highest weight loss and, thus, the highest purity of 99.05%.

In another study, Adebisi et al. [25] investigated the use of ash content of three agricultural wastes and showed the existence of biogenic silica and other complex hydroxides in the wastes that eventually transformed into complex silicates during calcination and volatilization, affecting the purity of the final products. The study also quantified the ash content of the biomasses 600, 700, and 800 °C to be 5.22, 6.10, and 7.01% of silicon dioxide, respectively. In this study, the extraction of silica from empty palm fruit bunch (EPFB) ash using calcination as the pretreatment step for the ash was performed. The ash and silica obtained were then characterized using XRD, XRF, TGA, SEM, and FTIR; and the results compared with those of the commercial silica.

2. Materials and Method

2.1. Materials

The sample used was obtained from Bayelsa Palm Oil mills in Southern Nigeria. EPFB-pyrolyzed ash was collected after the pyrolysis of the empty palm fruit bunches.

2.2. Methods

2.2.1. Calcination of EPFB Ash

The sieved EPFB ash was re-carbonized in a low-oxygen atmosphere at 600, 700, and 800 °C for 30 min at a heating rate of 30 °C/min in a closed muffle furnace before being stored dry to prevent aggregation. The physical properties of the ash considered included color and density. The compositional analysis of the samples was obtained using X-ray fluorescence (XRF). Morphology and elemental composition of the produced silica were checked with a scanning electron microscope equipped with energy dispersive X-ray (EDX).

2.2.2. Silica Extraction

The EPFB ash was washed in 1% HCl to remove impurities and then reacted with NaOH to precipitate the silica in the ash. The silica was extracted from the EPFB ash via co-precipitation using 1 M hydrochloric acid (HCl) as solvent and with 3 M NH_4OH precipitant. The mixture was agitated for 30 min at 50 °C on a hot plate equipped with a magnetic stirrer before filtration. The precipitated white solid particles after the reaction were allowed to cool down to room temperature. The solid residue was vacuum-filtered and washed repeatedly with distilled water until the washed water was at a pH of 7.1–7.3. The product was dried for 3 h at 110 °C in an oven and calcined in an air-steam oven at 550 °C for 3 h at a heating rate of 5 °C/min using a muffle furnace. Then the calcined solid was ground to a fine powder.

2.3. Analysis of EPFB Biomass Weight Loss

Weight loss analysis was performed to quantify the level of contaminants removed from the EPFB biomass samples after the washing and calcination operations, showing the mass of incombustible silica remaining in the waste samples. It was observed that the weight loss after combustion corresponded to the silica content in the sample. Equation (1) was used to obtain the weight loss of EPFB-ash-derived silica.

$$Weight\ loss = \frac{M_1 - M_2}{M_1} \times 100\% \tag{1}$$

where M_1 and M_2 represent the sample mass before and after the combustion, respectively, after six hours of calcination.

Characterization of EPFB Ash and Produced Silica

The non-destructive X-ray diffraction (XRD) technique was used to identify the crystalline phases, orientation, and determine their structural properties. The XRD patterns were obtained using a Bruker D2 Phaser Diffractometer with a data range of 2θ from 10 to 80°. A Carl Zeiss Sigma scanning electron microscope was used to understand the morphology of the materials. SEM images and microstructures of EPFB ash were recorded with an acceleration voltage of 5 kV.

A composition study was carried out to determine the presence of SiO_2 in the EPFB ash samples using a PANalytical X-ray fluorescence spectrometer (XRF). The particle size of the EPFB ash was examined through dynamic light scattering with a 532 nm laser (Mastersizer 2000). The textural property of the ash was obtained via N_2 physisorption at 77 K according to the Brunauer–Emmett–Teller (BET) method using an automatic gas adsorption analyzer at −195 °C in the range of relative pressures from 0.05 to 0.25. Autosorb was used to calculate the ash-specific surface area, pore volume, and average pore size. The total pore volume is given by $P/P_o = 0.995$. The micropore volume was calculated using

the t-plot method. EPFB ash. Surface chemistry of the produced silica was observed using an FTIR spectrophotometer (Perkin-Elmer, PC1600, Waltham, MA, USA) with a spectral range of 400–4000 cm^{-1}. At the same time, thermogravimetric analysis (TGA) was used in a thermal analysis system to analyze the physical and chemical phenomena related to the mass loss of EPFB biomass with temperature.

3. Results and Discussion

3.1. Mass Loss of EPFB Biomass at Different Temperatures after Calcination

Table 1 illustrates the weight loss in the samples following extraction with NaOH and H$_2$SO$_4$. The yield of silica, obtained using Equation (2), from the EPFB ash carbonization and extraction process based on the weight of the dry ash was 14.7–17.3%.

$$Silica\ Yield(\%) = \frac{Weight\ of\ silica}{Weight\ of\ EPFB\ ash} \times 100 \qquad (2)$$

Table 1. Mass loss of EPFB biomass at different temperatures after calcination.

Temperature °C	Before Calcination (g)	After Calcination (g)	Weight Loss (%)
600	15	2.6	82.7
700	15	2.2	85.3
800	15	2.4	84.0

The loss of yield could have been due to the washing and transfer of samples during the silica synthesis [30–32]. Claoston et al. [33] reported values in the 20–45% range above the values observed in this work. The weight loss of EPFB-pyrolyzed ash calcined at 700 and 800 °C was higher than that of ash burned at 600 °C as shown in TGA plot (Figure 1). The ash calcined at 600 °C, conversely, contained more organic components, volatile chemicals, and reactive water. The rest of the ash was mainly silica, which cannot be burned as fuel.
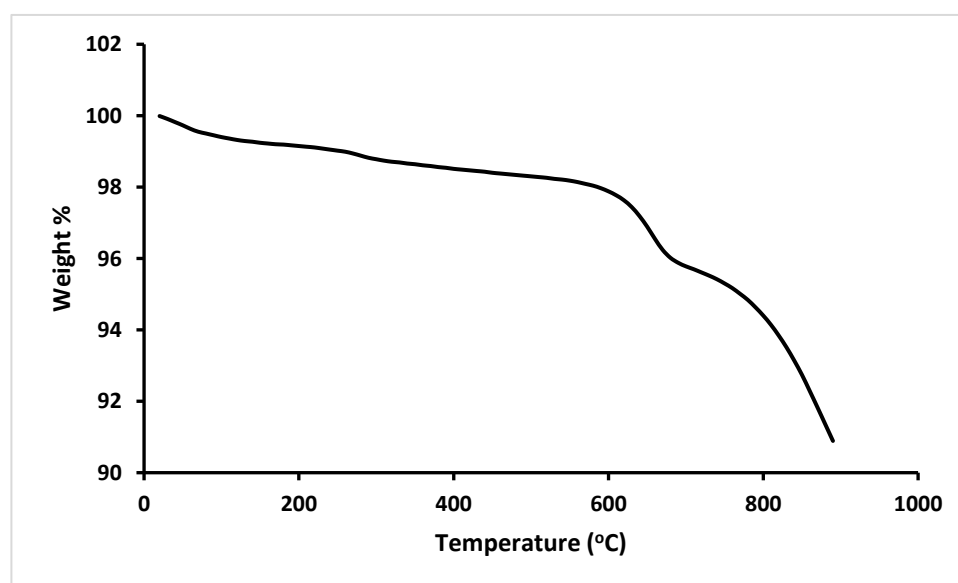

Figure 1. Thermogravimetric analysis (TGA) profile of the EPFB ash.

3.2. Textural Property and N$_2$ Adsorption Isotherm of EPFB Ash

Table 2 provides a summary of the textural property of the calcined EPFB ash. The table shows the BET surface area, the total volume of the pores, the pore size of the EPFB ash determined based on the N$_2$ adsorption-desorption isotherms (Figure 2) following the BET method, carried out at a calcination temperature of 800 °C. The ash's adsorption-desorption isotherm displayed a type-I isotherm, which is typical of microporous materials and shows

that nitrogen uptake increased swiftly via adsorption at external surfaces and micropores at low relative pressures (P/P$_0$) [34,35]. After the monolayer adsorption at low P/P$_0$, the nitrogen uptake was nearly constant, and the adsorption-desorption curves formed a small hysteresis loop at high relative pressure. The hysteresis in adsorption-desorption curves suggested some narrow mesopores in the ash [34]. A higher calcination temperature brought a change in the textural property and morphology of the ash, in which the surface area and pore volume increased with increasing calcination temperature. The ash sample had a high percentage of micropores, obtained by subtracting the mesopore and the external surface area from the total surface area given by the BET area (S$_{BET}$), suggesting that there were many broad microporous carbons and tiny mesopores. The results for calcination obtained in this work compared effectively to that of Ibrahim et al. [31] and Yang et al. [36] for, who considered when the surface enlargement could reach up to 80%. The pore diameter and volume data indicated that the ash had dominant microporous structures.

Table 2. Surface properties of calcined EPFB ash at various temperatures.

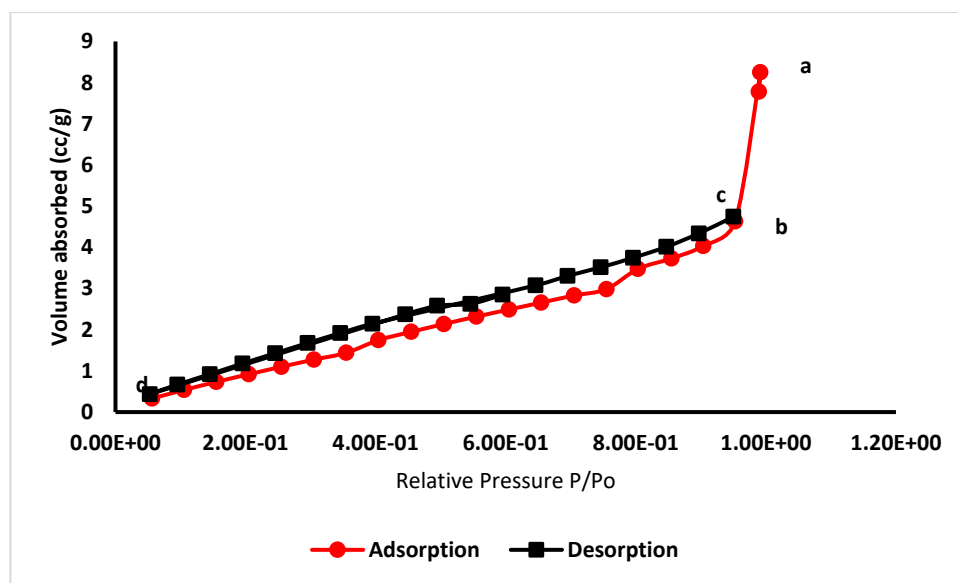| Temperature °C	BET Surface Area (m^2/g)	Total Pore Volume (cm^3/g)	Micropore Volume (cm^3/g)	Average Pore Size (Å)
600	91	0.02	0.007	83.66
700	580	0.10	0.060	25.08
800	921	0.24	0.170	20.86

Figure 2. Absorption/desorption isotherm of N$_2$ on EPFB ash. Line (a–d) correspond to the adsorption branch while line b-d to the desorption branch.

For the ash calcined at 800 °C the isotherm in Figure 2 showing the adsorption-desorption behavior is shown to possess a type IV isotherm indicative of a microporous material in which a hysteresis loop can be detected according to the IUPAC (International Union of Pure and Applied Chemistry) classification [35]. The upper portion (b-d) of the loop is the desorption zone, while the lower portion (a-d) is the adsorption zone. The adsorption isotherm (d-b) directly crossed the line that extended up to P/P$_o$ = 1. Accordingly, the adsorption behaviour of the ash shows a Type IV isotherm, indicating a mesoporous material [37]. In the low relative pressure range, the adsorbed volumes grew significantly, as seen in the initial stage. Most of the nitrogen molecules were therefore adsorbed into the microporous structure. At higher temperatures, the walls between two adjacent pores gets damaged, causing the existing pores to be strengthened and extended, forming new porosities with more extensive surface areas and smaller pore diameters, enabling easy adsorption onto the materials. The sample had a large fraction of

micropores, indicating a larger volume of broad microporous carbon and the presence of small mesopores.

The textural property of the produced silica from the EPFB ash in comparison with that of the commercial silica is presented in Table 3. The disparity in the BET surface area of the commercial silica (0.92 m^2 g^{-1}) in comparison with that of the silica produced from EPFB ash (0.38 m^2 g^{-1}) could be attributed to the complete removal of organic matter and impurities in the commercial silica [38]. Moreover, the commercial silica has a lower mean pore size (19.97 μm) than the mean pore size (23.9 μm) of silica produced from EPFB ash but a higher specific weight or density (2.69 kg/m^3) than that of the produced silica from EPFB ash (2.27 kg/m^3). The average pore size of the silica obtained from the EPFB ash, which is about 23.9 μm, indicates that the produced silica is mesoporous [38,39]. Generally, the EPFB ash, the produced silica from it and commercial silica exhibited similar characteristics, indicating that EPFB ash may be useful in the production of biogenic silica.

Table 3. Properties of EPFB ash compared to the produced silica and commercial silica.

Property	EPFB Ash	EPFB Silica	Commercial Silica *
Mean pore size (μm)	5.2	23.9	19.97
Specific weight/density (kg/m^3)	7.18	2.27	2.69
Surface area (m^2 g^{-1})	3.85	0.38	0.92
SiO$_2$ (%)	29.5	59.85	99.24
Morphology	Amorphous	Amorphous	Crystalline

* Source = [40].

3.3. X-ray Fluorescence (XRF) Analysis

Table 4 shows the chemical composition (%) of the samples and the coexistence of oxides such as SiO$_2$, CaO, Al$_2$O$_3$, and K$_2$O in the ash. As shown in the table, the level of SiO$_2$ in EPFB ash, determined by EDS at the various calcination temperature was in the range of 25% to 60%, with no significant trends observed in the calcination temperatures. Previous studies including Bhardwaj et al. [41], Gomesa et al. [42] and Van et al. [43] reported the presence of silica (SiO$_2$) as (92.81%), (86.0%) and (87.4%) respectively in agricultural waste ash with small quantities of other metallic and non-metallic oxides. The main metallic impurities identified in the EPFB ash were calcium, iron, potassium, magnesium, and phosphorus in concentrations of 7.34–15.72%, 1.55–13.74%, 10.36–11.66%, 8.62–8.73%, and 5.4–6.28%, respectively. The concentration of the impurities in the ash obtained were comparable to those reported in the literature using other analytical techniques such as EDTA complexometric titration [3,44]. The wide variation in the concentrations of the impurities with those found in literature can be attributed to factors such as palm species, climatic differences, type of soil, and use of fertilizers [45].

Acid leaching was used to remove these metals from the produced silica, and due to the low carbon content in the EPFB ash at 800 °C, the samples were slightly white and were preferred to the ash obtained at 600 and 700 °C. SiO$_2$ increased to 90% while the level of impurities decreased, revealing that the extraction of silica from EPFB ash is more effectively carried out through chemical treatment. The other elements in the ash, except for SiO$_2$, were dissolved in acid with reference to Fernandes et al. [40].

### 3.4. XRD Analysis of EPFB Ash and Produced Silica

The phase identification in the EPFB-ash-produced silica and commercial silica was assessed by observing the typical reflectance of spectral peaks at 2θ degrees produced when materials containing certain crystals are analyzed with XRD. The X-ray diffraction pattern of EPFB ash at three different temperatures (600, 700, and 800 °C) analyzed via XRD with a wavelength of CuKα = 1.540 Å at a rate of 2°/min in the angle range of 2θ = 5 − 80° determined the diffraction pattern, the crystal structure, and the particle size of the ash and extracted silica.

Table 4. % Elemental compositions of EPFB-derived silica at various calcination temperatures compared to commercial silica.

Oxides of Element	600 °C	700 °C	800 °C	Commercial Silica *
SiO_2	25.4	39.97	59.85	99.24
CaO	13.33	15.72	7.34	0.1147
K_2O	7.41	10.36	11.66	0.38
Al_2O_3	8.27	1.73	1.97	0.68
Fe_2O_3	15.84	13.74	1.55	-
P_2O_5	-	5.40	6.28	0.0244
MnO	0.51	0.38	0.44	0.0072
MgO	4.25	8.73	8.62	-
Na_2O	0.31	0.83	0.56	-
TiO_2	1.59	0.21	0.15	-
Cr_2O_3	0.15	0.07	0.06	-
Pb	-	-	-	0.0002
Mo	-	-	-	0.0006
LOI	5.2	1.16	0.95	<4

* Data for commercial silica was taken from Fernandes et al. [40].

At calcination temperatures above 700 °C, the SiO_2 in EPFB ash would consist phases of cristobalite and some tridymite because of the melting of the surfaces of ash silica and bonding of particles together [34]. This behavior was demonstrated in the calcination applied here and the ash was in crystalline form according to its XRD spectrum (Figure 3) with clearly defined Bragg's peaks at 2θ value of 30° and sharp peaks at several 2θ degrees due to the presence of crystalline quartz. The sharp quartz peak in the ash was converted to an amorphous silica solid due to the thermochemical process [46]. The XRD patterns of the extracted and commercial silica are shown in Figure 4. The silica derived from EPFB ash was inherently amorphous, as indicated by the large hump at the diffraction angle 2θ between 33 and 35°, confirming the amorphous nature of the silica [29].
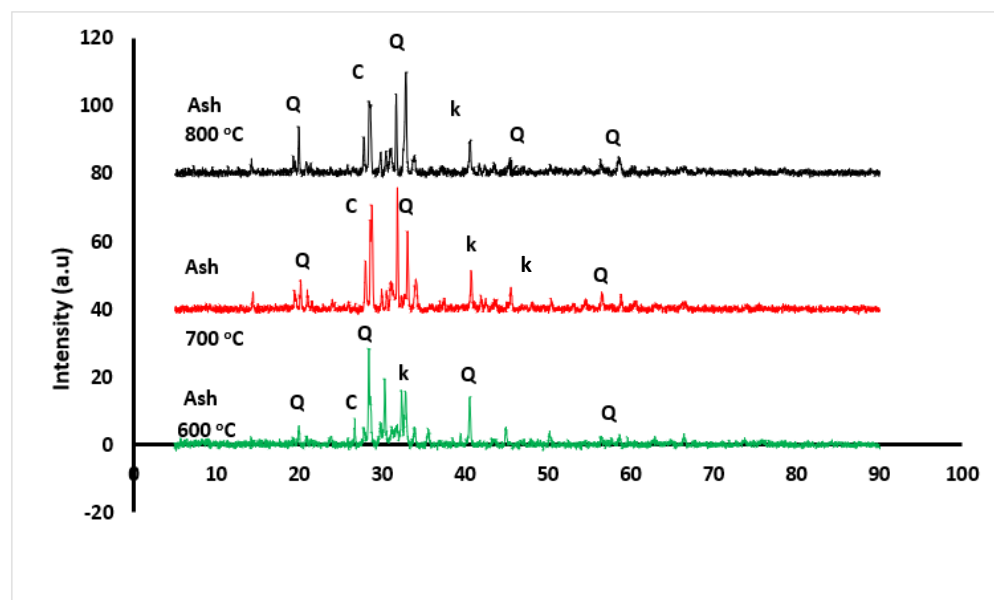
Q= Silica (SiO_4), k = $KalSiO_4$ and C = calcium carbonate ($CaCO_3$)

Figure 3. XRD pattern of the EPFB ash at various calcination temperatures.
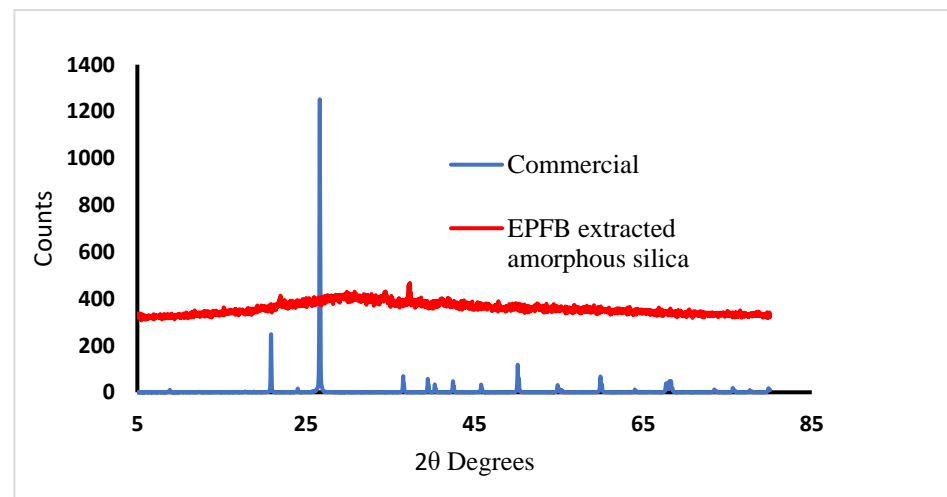
Figure 4. XRD pattern of produced silica and commercial silica.

In all the EPFB ash samples, the major components were Si, Al, K, Mg, Ca, and P, but the silica concentration was higher in the 800 °C sample than in the 700 and 600 °C samples. The XRD peak of the EPFB ash derived silica at 2θ value of 31.8° indicates silica in amorphous form (Figure 4). The silica XRD patterns resembled the common SiO_2 gel made from EPFB ash, as reported for palm kernel shell [27]. This is also consistent with similar XRD patterns of amorphous silica obtained from corn cob [27], rice husk [40], sugarcane bagasse [25], palm kernel shell [47], cassava periderm [28], and commercial amorphous silica gel [29].

3.5. Surface Morphology Analysis

The morphological structures and percentages of elements in the EPFB ash and extracted silica were examined using a scanning electron microscope (SEM) in conjunction with Energy-Dispersive Spectroscopy (EDS). Figures 5 and 6 show the morphology (SEM images) of the surface structure of the EPFB ash, which was produced at a calcination temperature of 800 °C, and the extracted silica at a scanned magnification of 25 and 10 μm. Irregular geometries such as cylindrical, flaky, angular porous, and spongy structures grouped into spherical clusters were recognized.
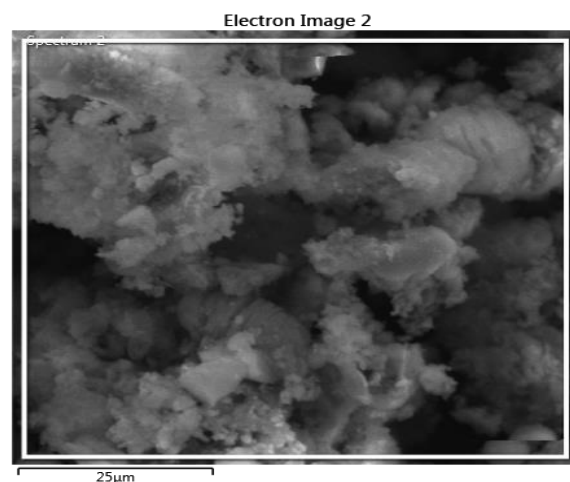

Figure 5. SEM micrograph of silica extracted from EPFB ash.
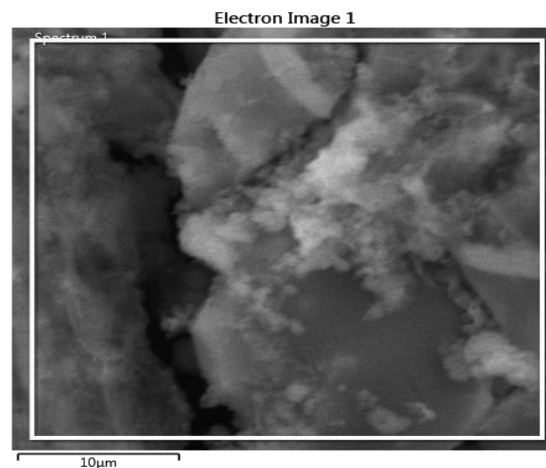
Figure 6. SEM micrograph of EPFB ash calcined at 800 °C.

The SEM images (Figure 5) generally showed irregular shapes with particle sizes of around 200 nm, which were believed to be silica. Many of these silica bodies were found embedded on the surface of the ash and the extracted silica, and agreed with the literature [13]. The SEM micrograph of the produced SiO_2 shows that the particles were irregular in shape. Awadh and Yaseen [48] reported similar irregular shape for silica obtained from rice husk ash and the authors attribiuted it to agglomeration. The amount of silica in the ash was 29.5% with some metallic impurities and 45.1% for the extracted silica as shown in Figure 6. The shape of the extracted silica were irregular with agglomerated particles. The EDS peaks for the extracted silica mainly contained Si and O elements. At the same time, the ash showed prominent Si and O peaks (Figure 7) with several other metallic impurities, as shown in Table 5. The elemental composition and phases of silica and ash calcined at 800 °C are shown in Figures 7 and 8. The presence of unburned particles, such as carbon, in the sample, was indicated by the formation of a crystalline structure.
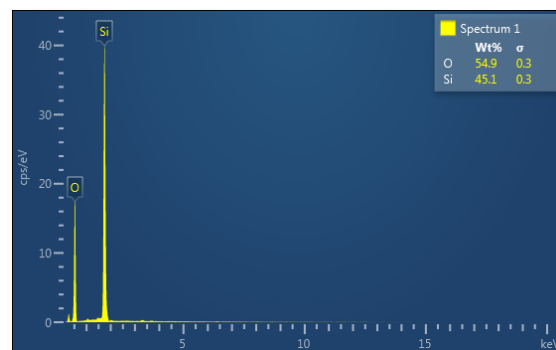

Figure 7. EDX graph of extracted silica.

Table 5. Elemental composition of ash and extracted silica.

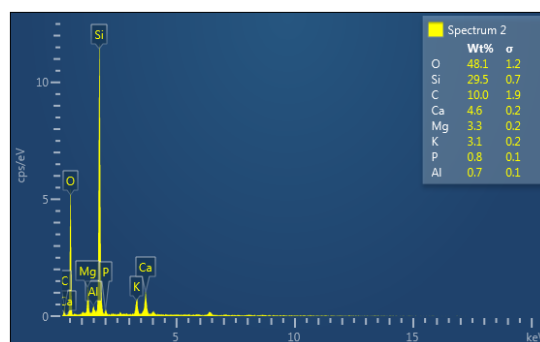| Elements	Peak (keV)	Ash at 800 °C (wt%)	Extracted Silica (wt%)
Si	0.05	29.5	45.1
O	1.75	48.1	54.9
C	0.025	10	-
Ca	3.74	4.6	-
Mg	1.84	3.3	-
K	3.47	3.1	-
P	2.00	0.8	-
Al	1.5	0.7	

Figure 8. EDX graph of EPFB ash produced at 800 °C.

3.6. FTIR Identification of Functional Groups in Silica

The observations show that the probability of finding silica in EPFB ash strongly depends on the presence of precursor silica groups in the sample. FTIR was used to assess the functional groups contained in the synthesized and commercial silica, as shown in Figure 9. At the same time, Table 6 summarizes the peak data of the dominant groups identified with the silica bond, including CH interaction and the OH groups in the silica. The generated silica's most significant IR absorption band was detected between 619 cm^{-1} and 1151 cm^{-1}. FTIR spectra of EPFB waste biomass ash, the EPFB ash derived, and the commercial silica in the range of 450–4000 cm^{-1} are shown in Figure 9. The most significant IR absorption band in the EPFB-ash-generated silica was detected between 619 cm^{-1} and 1151 cm^{-1}. A band at 797 cm^{-1} was designated as Si–O, which was sharp in the commercial silica sample. At the same time, the peak intensity decreased in EPFB-pyrolyzed ash-derived silica, and the EPFB ash was present in all the materials with little shifts in band location. A band at 1089 cm^{-1} presented in all the samples was due to TO4 (tetrahedral) of Al–Si, which indicated the presence of clinoptilolite (Na, K, Ca)$_2$–3Al$_3$(Al, Si)$_2$Si$_{13}$O$_{36}$12H$_2$-O) [49]. The crystalline absorption band at 1069, 1085, and 913 cm^{-1} was due to the asymmetric Si-O-Si mode of siloxane in EPFB silica, commercial silica, and EPFB ash and was associated with the stretching, bending, or deformation of the Si-O bond according to Sritham and Gunasekaran [50] and Osman and Sapawe, [51]. Similar absorption bands at 1064 cm^{-1}, 1086 cm^{-1}, and 1100 cm^{-1} have also been found by other researchers, including Awadh and Yaseen [48] and Osman and Sapawe [51]; these bands were assigned to Si-O-Si stretching. The siloxane-induced band at 913 cm^{-1} in EPFB ash changed to a higher frequency of 1069 cm^{-1} in the derived silica, indicating silica activity [46]. The stretching vibration of the Si-O bond and the tetrahedral coordination of amorphous silicon dioxide caused a strong peak at 1151 cm^{-1} [46]. Si-OH (OH groups) had a broadband range of 1620 to 1700 cm^{-1} in the ash and silica matrix [48]; however, there was no band detection at 1450–3450 cm^{-1} in all materials, suggesting the removal of all traces of water molecules and polar functional groups during the calcination process [52].

Table 6. Summary of the peak data of the dominant groups in EPFB ash, produced silica and commercial silica.

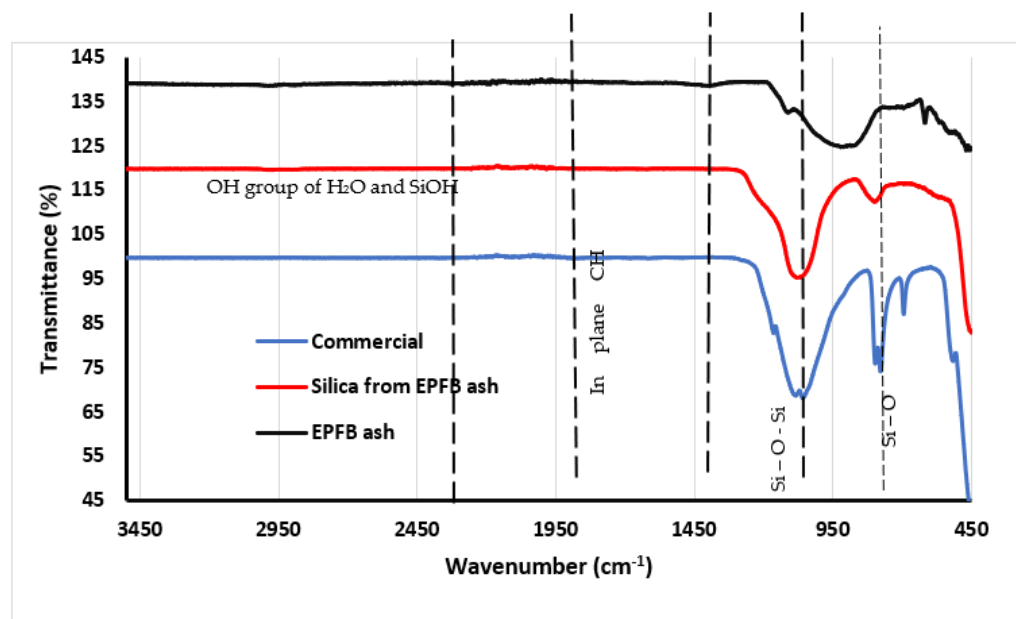| Wave Number	Compound
516–767	Si-O bond
1000–1058	Si-O-Si asymmetric bond stretching vibration
1720–2159	In-plane C=H bond
1998–2096	OH groups of Si-OH
2841–3000	OH stretching (H$_2$O) and hydroxyl (Si-OH)

Figure 9. FTIR spectra for EPFB-ash-generated silica and commercial silica.

The IR spectrum of the ash and the produced SiO_2, demonstrates the presence of all the vibrational bands of Si-OH, O—Si—O and Si—O—Si typical of amorphous SiO_2. The results of the absorption peak for the ash and commercial silica differed slightly to the EPFB-ash-extracted silica. The absorption pattern of the commercial silica had peaks representing SiO_2 functional groups at 1058 cm^{-1} (the stretching vibration of the Si-O group), 695 cm^{-1} (symmetrical stretching modes of the Si-O-Si), and 1150.86 cm^{-1} (absorption symmetric stretching modes of Si-O-Si) wavenumbers.

4. Conclusions

The calcination of EPFB biomass ash as a pretreatment step to producing silica, which could be applied in bio-oil upgrading, is demonstrated in this study. There has been extensive study on the effects of calcination temperature (600–800 °C) on the properties of silica formed from EPFB-pyrolyzed ash. The resulting silica had a tiny crystal size (43 nm) and a strong basicity according to the results obtained by lowering the calcination temperature (600 °C). As the calcination temperature rose from 600 °C to 800 °C, the amount of acid in the bio-oil dramatically increased from 17.89% to 32.30%. The amount of impurities in the silica significantly dropped from 11.47% to 5.21%, showing improved silica quality. In general, the formation of silica is more advantageous at an 800 °C calcination temperature. We effectively extracted amorphous silica (SiO_2) from pyrolyzed EPFB waste ash in the final step of the process. The potential for silica in manufacturing catalysts for bio-oil upgrading was evaluated by comparing its characteristics with that of commercial silica. Accordingly, the weight loss in the sample represented the quantity of silica present in the ash, with lower temperatures carrying somewhat less silica than the ash calcined at 800 °C. The production of porous and amorphous silica from pyrolyzed ash of empty palm bunch biomass is evidence that simple calcination processes and acid leaching could obtain silica with a purity of over 98 percent. Synthetic silica offers a lot of potential for application in the production of zeolite catalysts for use in upgrading bio-oil.

References

1. Alves, C.; Valk, M.; de Jong, S.; Bonomi, A.; van der Wielen, L.; Mussatto, S. Techno-economic assessment of biorefinery technologies for aviation biofuels supply chains in Brazil. *Biofuels Bioprod. Biorefining* **2017**, *11*, 67–91. [CrossRef]
2. Wang, J.; Bi, P.; Zhang, Y.; Xue, H.; Jiang, P.; Wu, X. Preparation of jet fuel range hydrocarbons by catalytic transformation of bio-oil derived from fast pyrolysis of straw stalk. *Energy* **2015**, *86*, 488–499. [CrossRef]
3. Arfiana, E.; Finali, R.; Noor, I.; Murti, S.S.; Suratno, H.; Rosyadi, E.; Saputra, H.; Noda, R. Oil palm empty fruit bunch ash as a potassium source in the synthesis of NPK fertilizer. *IOP Conf. Ser. Earth Environ. Sci.* **2021**, *749*, 012038. [CrossRef]
4. Madrid, R.; Nogueira, C.; Margarido, F. Production and characterization of amorphous silica from rice husk waste. In Proceedings of the WasteEng'2012: 4th International Conference on Engineering for Waste and Biomass Valorisation, Porto, Portugal, 10–13 September 2012.
5. Pérez-Botella, E.; Valencia, S.; Rey, F. Zeolites in Adsorption Processes: State of the Art and Future Prospects. *Chem. Rev.* **2022**, *122*, 17647–17695. [CrossRef]
6. Zaffar, S.; Kumar, A.; Memon, N.; Kumar, R.; Saand, A. Investigating Optimum Conditions for Developing Pozzolanic Ashes from Organic Wastes as Cement Replacing Materials. *Materials* **2022**, *15*, 2320. [CrossRef] [PubMed]
7. Future Market Insights, Inc. *Worldwide Demand for Precipitated Silica Market Will Surge at a Robust 8.8% CAGR during 2022 and 2032*; Globe Newswire: Newark, NJ, USA, 2023.
8. Kaniapan, S.; Hassan, S.; Ya, H.; Nesan, K.P.; Azeem, M. The Utilisation of Palm Oil and Oil Palm Residues and the Related Challenges as a Sustainable Alternative in Biofuel, Bioenergy, and Transportation Sector: A Review. *Sustainability* **2021**, *13*, 311. [CrossRef]
9. Elanthikkal, S.; Mohamed, H.; Alomair, N. Green Route Synthesis of Amorphous Silica from Oil Palm Decanter Cake: From Literature Review to Experiments. *Indones. J. Sci. Technol.* **2023**, *8*, 141–156.
10. Bakar, R.; Yahya, R.; Gan, S. Production of high purity amorphous silica from rice husk. *Procedia Chem.* **2016**, *19*, 189–195. [CrossRef]
11. Suryana, R.; Iriani, Y.; Nurosyid, F.; Fasquelle, D. Characteristics of silica rice husk ash from Mojogedang Karanganyar Indonesia. *IOP Conf. Ser. Mater. Sci. Eng.* **2018**, *367*, 012008. [CrossRef]
12. Pa, F.; Chik, A.A.; Bari, M. Palm Ash as an Alternative Source for Silica Production. In *MATEC Web of Conferences*; EDP Sciences: Kangar, Malaysia, 2016.
13. Samat, N.; Zulkafly, S.; Jaman, U.; Zauzi, N.; Rahman, M.; Baini, R. Characteristics Analysis of Bio-Based Silica Extracted from. *Int. J. Eng. Technol.* **2018**, *7*, 94–96.
14. Rahmat, F.; Fen, Y.; Anuar, M.; Omar, N.; Zaid, M.; Matori, K.; Khaidir, R. Synthesis and Characterization of ZnO-SiO2 Composite Using Oil Palm Empty Fruit Bunch as a Potential Silica Source. *Molecules* **2021**, *26*, 1061. [CrossRef] [PubMed]
15. Affandi, S.; Setyawan, H.; Winardi, S.; Purwanto, A.; Balgis, R. A facile method for production of high-purity silica xerogels from bagasse ash. *Adv. Powder Technol.* **2009**, *20*, 468–472. [CrossRef]
16. Zang, J.; Yu, H.; Liu, G.; Hong, M.; Liu, J.; Chen, T. Research Progress on Modifications of Zeolite Y for Improved Catalytic Properties. *Inorganics* **2023**, *11*, 22. [CrossRef]
17. Permatasari, N.; Sucahya, T.; Nandiyanto, A. Review: Agricultural Wastes as a Source of Silica Material. *Indones. J. Sci. Technol.* **2016**, *1*, 82–106. [CrossRef]
18. Pandiangan, K.; Simanjuntak, W.; Hadi, S.; Ilim, I.; Amrulloh, H. Physical characteristics and utilization of ZSM-5 prepared from rice husk silica and aluminum hydroxide as catalyst for transesterification of Ricinus communis oil. *Mater. Res. Express* **2021**, *8*, 06550. [CrossRef]
19. Liu, Y.; Guo, Y.; Zhu, Y.; An, D.; Gao, W.; Wang, Z.; Ma, Y.; Wang, Z. A sustainable route for the preparation of activated carbon and silica from rice husk ash. *J. Hazard. Mater.* **2011**, *186*, 1314–1319. [CrossRef]
20. Costa, J.; Paranhos, C. Systematic evaluation of amorphous silica production from rice husk ashes. *J. Clean. Prod.* **2018**, *192*, 688–697. [CrossRef]
21. Velmurugan, P.; Shim, J.; Lee, K.J.; Cho, M.; Lim, S.S.; Seo, S.K.; Cho, K.M.; Bang, S.K.; Oh, B.T. Extraction, characterization, and catalytic potential of amorphous silica from corn cobs by sol-gel method. *J. Ind. Eng. Chem.* **2015**, *29*, 298–303. [CrossRef]
22. Kaya, G.; Yilmaz, E.; Deveci, H. Sustainable nanocomposites of epoxy and silica xerogel synthesized from corn stalk ash: Enhanced thermal and acoustic insulation performance. *Compos. Part B Eng.* **2018**, *150*, 1–6. [CrossRef]

23. Usman, A.M.; Raji, A.; Waziri, N.H.; Hassan, M.A. A Study on silica and alumina potential of the savannah bagasse ash. *IOSR J. Mech. Civ. Eng.* **2014**, *11*, 48–52. [CrossRef]

24. Channoy, C.; Maneewan, S.; Punlek, C.; Chirarattananon, S. Preparation and characterization of silica gel from bagasse ash. *Adv. Mater. Res. Trans. Tech. Publ.* **2018**, *1145*, 44–48. [CrossRef]

25. Adebisi, A.; Agunsoye, J.; Bello, S.; Kolawole, F.; Ramakokovhu, M.; Hassan, S.; Daramola, M. Extraction of Silica from Sugarcane Bagasse, Cassava Periderm and Maize Stalk: Proximate Analysis and Physico-Chemical Properties of Wastes. *Waste Biomass Valor* **2019**, *10*, 617–629. [CrossRef]

26. Farirai, F.; Mupa, M.; Daramola, M. An improved method for the production of high purity silica from sugarcane bagasse ash obtained from bioethanol plant boiler. *Part. Sci. Technol.* **2021**, *39*, 252–259. [CrossRef]

27. Imoisili, P.; Ukoba, K.; Jen, T. Green technology extraction and characterisation of silica nanoparticles from palm kernel shell ash via sol–gel. *J. Matters Res. Technol.* **2020**, *9*, 307–313. [CrossRef]

28. Adebisi, J.A.; Agunsoye, J.O.; Bello, S.A.; Haris, M.; Ramakokovhu, M.M.; Daramola, M.O.; Hassan, S.B. Extraction of Silica from Cassava Periderm using Modified Sol-Gel Method. *Niger. J. Technol. Dev.* **2018**, *15*, 57–65. [CrossRef]

29. Utama, P.; Yamsaengsung, R.; Sangwichien, C. Silica gel derived from palm oil mill fly ash. *Songklanakarin J. Sci. Technol.* **2018**, *40*, 121–126.

30. Idris, J.; Shirai, Y.; Anduo, Y.; Ali, A.; Othman, M.; Ibrahim, I.; Husen, R.; Hassan, M. Improved yield and higher heating value of biochar from oil palm biomass at low retention time under self-sustained carbonization. *J. Clean. Prod.* **2015**, *104*, 475–479. [CrossRef]

31. Ibrahim, I.; Tsubota, T.; Hassan, M.; Andou, Y. Surface Functionalization of Biochar from Oil Palm Empty Fruit Bunch through Hydrothermal Process. *Processes* **2021**, *9*, 149. [CrossRef]

32. Akhayere, E.; Kavaz, D.; Vaseashta, A. Efficacy Studies of Silica Nanoparticles Synthesized Using Agricultural Waste for Mitigating Waterborne Contaminants. *Appl. Sci.* **2022**, *12*, 9279. [CrossRef]

33. Claoston, N.; Samsuri, A.; Husni, M.A.; Amran, M.M. Effects of pyrolysis temperature on the physicochemical properties of empty fruit bunch and rice husk biochars. *Waste Manag. Res.* **2014**, *32*, 331–339. [CrossRef]

34. Saceda, J.; de Leon, R.; Rintramee, K.; Prayoonpokarach, S. Properties of silica from rice husk and rice husk ash and their utilization for zeolite y synthesis. *Quim. Nova* **2011**, *34*, 1394–1397. [CrossRef]

35. Aranovich, G.; Donohue, M. Adsorption isotherm for microsporous adsorbents. *Carbon* **1995**, *33*, 1369–1373. [CrossRef]

36. Yang, K.; Fox, J. Adsorption of humic acid by acid-modified granular activated carbon and powder activated carbon. *J. Environ. Eng.* **2018**, *144*, 04018104. [CrossRef]

37. Kurji, B.; Abba, A. Comparative Study of Textural Properties for Various Silica by Nitrogen Adsorption-desorption Technique. *Egypt. J. Chem.* **2022**, *65*, 313–320. [CrossRef]

38. Dhaneswara, D.; Fatriansyah, J.; Situmorang, F.; Haqoh, A. Synthesis of Amorphous Silica from Rice Husk Ash: Comparing HCl and CH_3COOH Acidification Methods and Various Alkaline Concentrations. *Int. J. Technol.* **2020**, *11*, 200–208. [CrossRef]

39. Bonyadi, Z.; Kumar, P.; Foroutan, R.; Kafaei, R.; Arfaeinia, H.; Farjadfard, S.; Ramavandi, B. Ultrasonicassisted synthesis of Populus alba activated carbon for water defluorination: Application for real wastewater. *Korean J. Chem. Eng.* **2019**, *36*, 1595–1603. [CrossRef]

40. Fernandes, I.; Calheiro, D.; Sánchezb, F.; Camachob, A.; Rochac, T.; Caldas de Sousaa, V. Characterization of Silica Produced from Rice Husk Ash: Comparison of Purification and Processing Methods. *Mater. Res.* **2017**, *20*, 512–518. [CrossRef]

41. Bhardwaj, A.; Hossain, S.; Majhi, M. Preparation and characterization of clay bonded high strength silica refractory by utilizing agriculture waste. *Bol. Soc. Esp. Cerám. Vidr.* **2017**, *56*, 256–262. [CrossRef]

42. Gomesa, G.; Philipssenc, C.; Barda, E. Rice husk bubbling fluidized bed combustion for amorphous silica synthesis. *J. Environ. Chem. Eng.* **2016**, *4*, 2278–22906. [CrossRef]

43. Van, V.; Rößler, C.; Bui, D. Pozzolanic reactivity of mesoporous amorphous rice husk ash in portlandite solution. *Constr. Build. Mater.* **2014**, *59*, 111–119. [CrossRef]

44. Adu, M.O.; Atia, K.; Arthur, E.; Asare, P.; Obour, P.; Danso, E.; Frimpong, K.; Sanleri, K.; Asare-Larbi, S.; Adjei, R.; et al. The use of oil palm empty fruit bunches as a soil amendment to improve growth and yield of crops. A meta-analysis. *Agron. Sustain. Dev.* **2022**, *42*, 13. [CrossRef]

45. Lizcano-Toledo, R.; Reyes-Martín, M.; Celi, L.; Fernández-Ondoño, E. Phosphorus Dynamics in the Soil–Plant–Environment Relationship in Cropping Systems: A Review. *Appl. Sci.* **2021**, *11*, 11133. [CrossRef]

46. Sivakumar, G.; Amutha, K. Studies on silica obtained from cow dung ash. *Adv. Mater. Res.* **2012**, *584*, 470–473. [CrossRef]

47. Imoisili, P.; Ukoba, K.; Jen, T. Synthesis and characterization of amorphous mesoporous silica from palm kernel shell ash. *Bol. De La Soc. Esp. De Ceram. Yvidrio* **2020**, *59*, 159–164. [CrossRef]

48. Awadh, S.; Yaseen, Z. Investigation of silica polymorphs stratified in siliceous geode using FTIR and XRD methods. *Mater. Chem. Phys.* **2019**, *228*, 45–50. [CrossRef]

49. Chen, X.; Li, S.; Chen, W.; Chen, Y.; Chen, H.; Yang, H. Influence of calcination temperature on calcined carbide slag assisted biomass pyrolysis. *Fuel Process. Technol.* **2022**, *234*, 107339. [CrossRef]

50. Sritham, E.; Gunasekaran, S. FTIR spectroscopic evaluation of sucrose-maltodextrin-sodium citrate bioglass. *Food Hydrocoll.* **2017**, *70*, 371–382. [CrossRef]

51. Osman, N.; Sapawe, N. Synthesis of silica (SiO$_2$) from reproducible acid-leached oil palm frond ash (OPFA) via optimized sol–gel method. *Mater. Today Proc.* **2020**, *31*, 249–252. [CrossRef]
52. Usman, A.; Abduljabbar, A.; Vithanage, M.; Ok, Y.; Ahmad, M.; Ahmad, M. Biochar production from date palm waste: Charring temperature induced changes in composition and surface chemistry. *J. Anal. Appl. Pyrolysis* **2015**, *115*, 392–400. [CrossRef]